Mon. Not. R. Astron. Soc. **000**, 1–?? (2008) Printed 13 February 2009 (MN LATEX style file v2.2)

Metallicities and ages of stellar populations at a high Galactic latitude field

Michael H. Siegel, [1⋆] Yüksel Karataş[2]† and I. Neill Reid[3]‡
[1] *Pennsylvania State University, 525 Davey Laboratory, State College, PA, 16801, USA*
[2] *Istanbul University Science Faculty, Department of Astronomy and Space Sciences, 34119 University-Istanbul, Turkey*
[3] *Space Telescope Science Institute, 3700 San Martin Drive, Baltimore, MD, 21218, USA*

Accepted. Received; in original form

ABSTRACT
We present an analysis of $UBVRI$ data from the Selected Area SA 141. By applying recalibrated methods of measuring ultraviolet excess (UVX), we approximate abundances and absolute magnitudes for 368 stars over 1.3 square degrees out to distances over 10 kpc. With the density distribution constrained from our previous photometric parallax investigations and with sufficient accounting for the metallicity bias in the UVX method, we are able to compare the vertical abundance distribution to those measured in previous studies. We find that the abundance distribution has an underlying uniform component consistent with previous spectroscopic results that posit a monometallic thick disk and halo with abundances of $[Fe/H] = -0.8$ and -1.4, respectively. However, there are a number of outlying data points that may indicate contamination by more metal-rich halo streams. The absence of vertical abundance gradients in the Galactic stellar populations and the possible presence of interloping halo streams would be consistent with expectations from merger models of Galaxy formation. We find that our UVX method has limited sensitivity in exploring the metallicity distribution of the distant Galactic halo, owing to the poor constraint on the UBV properties of very metal-poor stars. The derivation of metallicities from broadband UBV photometry remains fundamentally sound for the exploration of the halo but is in need of both improved calibration and superior data.

Key words:
stars: abundances, stars: Population II, Galaxy: evolution

1 INTRODUCTION

The three-dimensional abundance distribution of the Milky Way field stars is a key constraint on models of Galactic formation (see, e.g., the reviews in Majewski et al. 1993; Freeman & Bland-Hawthorn 2002). The observed abundance distribution is the convolution of the enrichment history of the Milky Way and the dynamical evolution of its stellar populations (as reflected in their spatial and kinematical distributions). Specific models of galaxy formation make specific predictions about the abundance distribution measured *in situ* from the field stars that can be tested against large catalogues of abundance measures. For example, the hypothesis that the Galactic halo was formed in a global collapse was primarily supported by stars on more radial orbits (and therefore reaching higher z heights above the Galactic midplane) being more metal-poor than stars on planar orbits (Eggen, Lynden-Bell & Sandage 1962). However, the global collapse theory was unable to account for the lack of an abundance gradient in the Milky Way globular clusters (Searle & Zinn 1978), leading to the hypothesis that the Galaxy formed at least partly through the merging of larger systems – a hypothesis now well-supported by studies of stellar kinematics and spatial distributions (Majewski, Munn & Hawley 1996; Ivezic et al. 2000; Yanny et al. 2000; Vivas et al. 2001; Siegel et al. 2002, hereafter S02; Newberg et al. 2002; Yanny et al. 2003; Majewski et al. 2003; Rocha-Pinto et al. 2004; Belokurov et al. 2006; Grillmair et al. 2006; Vivas & Zinn 2006; Juric et al. 2008) as well as the properties of globular clusters (see, e.g., Marin-Franch et al. 2008).

The abundance distribution is of particular importance to understanding the nature of the Galactic thick disk. An abundance gradient in the thick disk would favor a scenario

⋆ E-mail:siegel@astro.psu.edu
† E-mail:karatas@istanbul.edu.tr
‡ E-mail:inr@stsci.edu

in which the thick disk was formed either in the slow late stages of the early Galactic collapse or the gradual kinematical diffusion of disk stars. On the other hand, a monometallic or irregular metallicity distribution among these stars would favor the thick disk having formed via the kinematical heating of an early thin disk or directly from merger debris.

The Galactic metallicity distribution is best probed directly through spectroscopic surveys (Yoss, Neese & Hartkopf 1987; Allende-Prieto et al. 2006, hereafter AP06). However, an alternative method to spectroscopy is the use of field star UBV photometry (Majewski 1992; Gilmore & Wyse 1985; Karaali et al. 2003). UBV photometry allows the measurement of approximate abundances because the ultraviolet flux of a star is dramatically affected by the line-blanketing of the star's heavy metals – a phenomenon first described by Roman (1954) and Wildey et al. (1962). The measurement of ultraviolet excess – the amount of "extra" ultraviolet light produced by metal-poor stars in comparison to metal-rich stars of similar spectral type – is necessarily less precise than spectroscopy. However, it has the advantage of allowing the simultaneous measurement of many more stars out to the magnitude limit of a photometric survey.

The photometric and spectroscopic studies referenced above have consistently shown vertical abundance gradients ranging from -0.75 to -0.08 dex kpc^{-1}, with the gradient slowly flattening at the high-z regions dominated by the halo. However, these gradients do not necessarily reflect abundance gradients *within* any Galactic population. They could also be produced by the transitions from one monometallic population to the other. Majewski (1992), for example, argues from a photometric and astrometric survey of the North Galactic Pole that the thick disk has no vertical metallicity gradient and a non-Gaussian metallicity distribution. AP06, using a spectroscopic survey of kinematically-selected stars, demonstrate that neither the thick disk nor the halo have an intrinsic vertical abundance gradient. They also find that while the halo has a broad range of abundances, the thick disk has a compact metallicity distribution with a peak metallicity of $[Fe/H] \sim -0.7$. Du et al. (2004), using an analysis of BATC photometry, posit that *all three* old stellar populations (old disk, thick disk and halo) lack a vertical abundance gradient.

As this paper was in preparation, Ivezic et al. (2008, hereafter I08) published an extensive study of ugr photometry taken from the Sloan Digital Sky Survey. The tremendous number of stars available allows them to probe both broad and fine structure in the abundance distribution. While they confirm the general properties of the Galactic populations depicted in earlier surveys such as AP06, they do so with much more precision. Remarkably, their results would be consistent with the complete absence of a thick disk in the Milky Way or its reduction to the Metal-Weak Thick Disk described by Norris (1987). Karatas et al. (2008) have also recently analyzed $ugriz$ photometry from the CFHTLS DR4. In contrast to other studies, they find a vertical abundance gradient in the halo.

In this paper, we present an analysis of stars in the Kapteyn Selected Area SA 141, which is located near the South Galactic Pole and is ideal for probing vertical spatial, kinematical and abundance distributions. Trefzger, Pel & Gabi (1995) previously studied the photometric properties of this field in an attempt to constraint the metallicity distribution. Using 112 stars over 1.9 square degrees to a depth of $V = 14.8$, Trefzger et al. found evidence for a distinct thick disk population and gradients roughly consistent with previous spectroscopic studies.

We now expand upon their result, presenting an analysis of photoelectric $UBVRI$ photometry in a similar field but to greater depth. The present study provides an independent check on the remarkable results of I08 as well as an exploration of issues affecting the derivation of metallicities from broadband UBV colours. Section 2 of this paper describes the observations, corrections for foreground extinction and removal of QSOs contamination. Section 3 describes the method used to measure photometric abundances, absolute magnitudes and distances while Section 4 shows our analysis of the abundance distribution perpendicular to the Galactic disk and the comparison of our measures to those expected from the most recent models.

2 OBSERVATION AND DATA REDUCTION

2.1 Photometric Data

The SA 141 field was observed as part of a larger starcounts survey, described in detail in S02. In brief, SA 141 was one of twelve fields observed in the $UBVRI$ passbands with the wide-field Cassegrain CCD camera on the 1-m Swope telescope at Las Campanas Observatory between 1993 and 1998. Each field was observed in a uniform grid of pointings. In the case of SA 141, the U data cover approximately 1.3 square degrees to a mean depth of $U \sim 21$. Transformation equations to the standard system of Landolt (1992) were derived through matrix inversion techniques and each field was iteratively transformed to this system. We applied the morphological object classification techniques of S02 and identified 1294 star-like objects with measurable U magnitudes.

Since the publication of S02, we have slightly improved the data, generating astrometry from the IRAF TFINDER program and USNO SA2.0 catalog (Monet al. 1996). We also combined stars with multiple observations and removed slight photometric inconsistencies between the individual pointings using techniques described in Siegel et al. (2009).

Photometry was de-reddened using the reddening maps and extinction coefficients of Schlegel, Finkbeiner & Davis (1998). Although several studies have indicated that the Schlegel maps over-estimated the reddening (see, e.g., Cambresy et al. 2005), the stars in the SA 141 field have minimal extinction ($0.011 \leqslant E(B-V) \leqslant 0.024$), minimizing any impact on our study.

2.2 QSO and galaxy contamination

Deep, high-latitude fields can suffer significant contamination from background galaxies. While SO2's morphological techniques effectively remove most diffuse galaxies, compact galaxies can remain in the sample (Reid et al. 1996; S02). Fortunately, UBV photometry provides an excellent secondary resource with which to remove compact background galaxies.

Figs. 1a and c show the $(U-B)_o$,$(B-V)_o$ and $(V-R)_o$,$(B-V)_o$ colour-colour diagrams of SA 141. The sample shows a very clear and narrow stellar locus but has

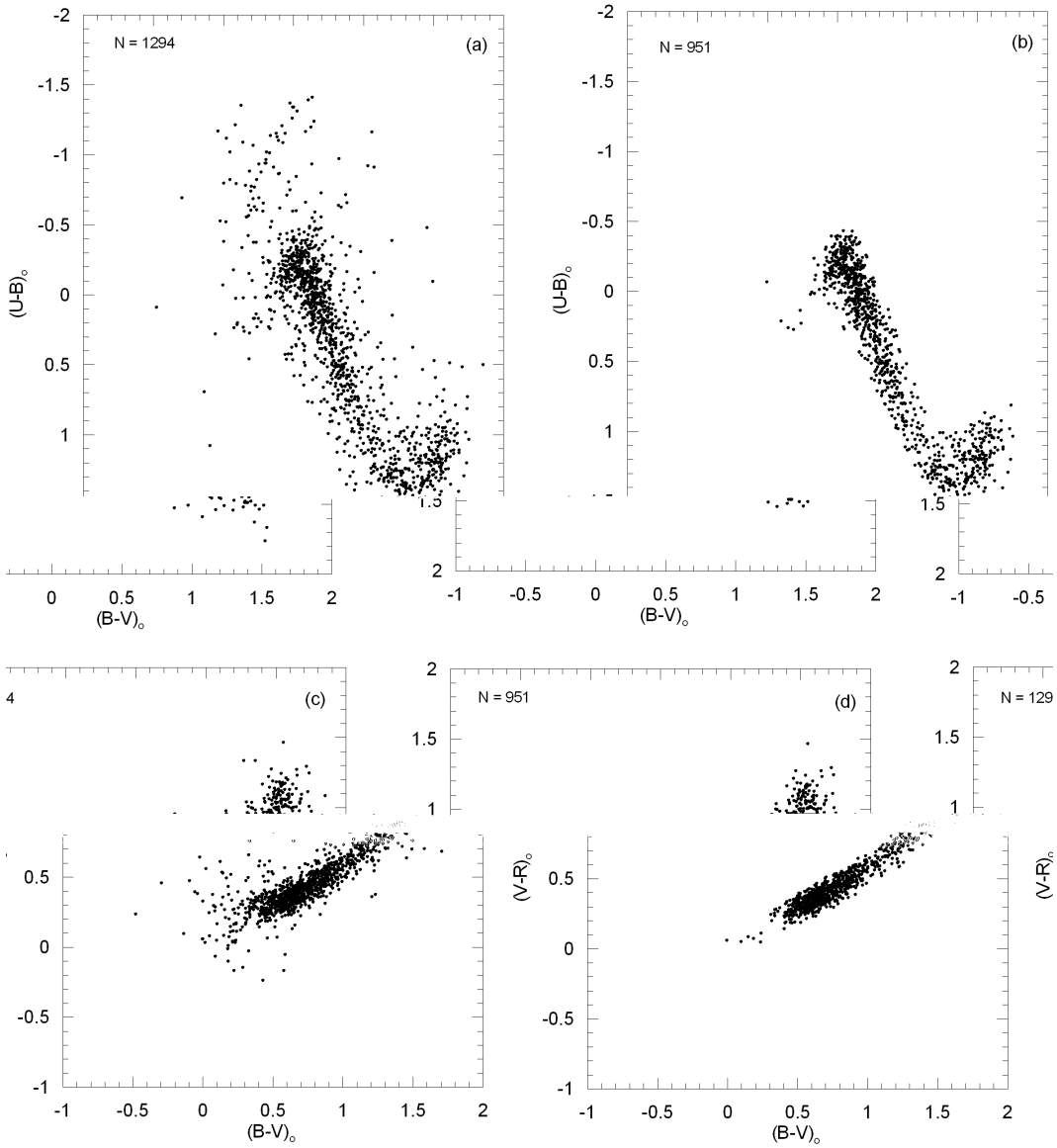

Figure 1. Colour-colour diagrams for SA 141 field stars. Left panels (a) and (c) show $(U-B)_o$,$(B-V)_o$ and $(V-R)_o$,$(B-V)_o$ two colour diagrams of 1294 stars and star-like objects. Right panels (b) and (d) show $(U-B)_o$, $(B-V)_o$ and $(V-R)_o$,$(B-V)_o$ diagrams for 951 stars after possible galaxies and quasars are eliminated.

significant contamination from compact galaxies and QSOs, manifested in the broader distribution overlying the narrow stellar locus. To remove these objects, we applied the selection criterion of Chen et al. (2001), which removes objects with $(u-g)_0 > 0.50$. This transforms to a $U-B$ colour of -0.48, using the equations of Smith et al. (2002). We further applied methods outlined in Fan et al. (1999) and Karaali et al. (2003), which remove objects based on their location relative to the dominant stellar colour−colour locus.

This cleaning reduced the sample from 1294 objects to 951 stars (Figs. 1b and d). The 343 objects removed from the sample is a far greater than the level of QSO contamination expected (see, e.g., Richards et al. 2001) and it is likely that our photometric locus method is removing outlier stars that have compromised measures or unusual properties. However, the objects removed from our analysis lie well outside the boundaries of the iso-metallicity lines discussed in Sect. 3.3 and their absence does not affect our analysis.

3 ANALYSIS TECHNIQUES

3.1 Stellar population types

The $(V_o, (B-V)_o)$ colour-magnitude diagram for the 951 stars in the SA141 sample is plotted in Figure 2. We have indicated the cut-off colour indices for thin and thick disks and halo populations as described by Chen et al. (2001, figure 6). These cutoffs occur at $(g-r)_0$ colours of 0.33 and 0.20, respectively, which we convert to $(B-V)_0$ colours of 0.54 and 0.40 using the transformation of Smith et al. (2002). Our photometric distribution is roughly consistent with Chen, with the thick disk dominating the starcounts

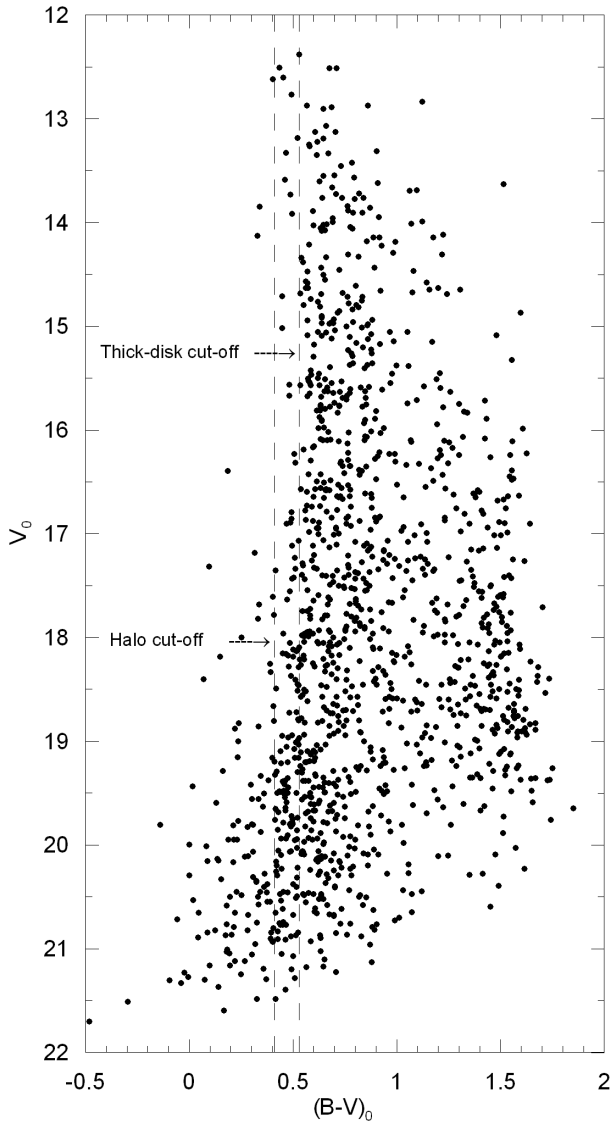

Figure 2. The $(B–V)_o - V_o$ colour-magnitude diagram of 951 stars in SA 141 field. Dashed lines show the cut-offs of $(B-V)_o$ for the thick disk and halo derived by Chen et al. (2001).

to about $V_0 \sim 19$ and the halo dominating at fainter magnitudes.

3.2 Model Comparison

Untangling stellar populations from raw colour-magnitude diagrams is a difficult process at best and frequently prone to degenerate solutions, especially when based upon observations in a single direction. Sophisticated models, which incorporate up-to-date spatial and abundance distributions, luminosity functions and isochrones, can be used to make Monte Carlo comparisons with which to constrain the properties of the underlying stellar populations. The most readily available and recently updated model is the Besancon model of stellar population synthesis (Robin et al. 2003, hereafter R03)[1], which can produce synthetic photometric catalogs based on an updated Galactic structure model and an input set of magnitude limits and error functions.

Figure 3 compares the Besancon simulation to the SA 141 photometry. For the simulation, we used the updated default structural parameters given by the Besancon simulator. We simulated errors using exponential distributions fit to the mean error locus of the data (Figure 4). No *a priori* color limits were included and the magnitude limit was set to the mean imaging limit of the SA141 data ($V = 21.2$; $B = 20.9$; $U = 21.0$). The imaging limit was defined in S02 as the faintest magnitude at which stars and galaxies could be distinguished based on DAOPHOT morphological parameters.

Both the real and simulated data fall along an arced locus in colour-colour space, with the location of each star being a function of its effective temperature and stellar metallicity (as explored in detail in Sect. 3.3). The numerous blue stars that create a clump in upper left corner of the colour-colour diagram would correspond to the blue edge depicted in Fig. 2 and shown in the lower panels of Fig. 3. The blue edge is comprised of intrinsically bright early-type stars. These stars are faint in the CMD and therefore several kpc distant in regions dominated by the metal-poor halo. The long trail of stars to redward is the increasing contribution of the intrinsically fainter (and therefore nearer) late-type stars, which would be in regions of the Galaxy dominated by the thick and thin disks.

While the basic features are similar, a number of discrepancies are seen. The simulated blue edge is much more populous than the observed blue edge. The simulated blue edge also has a much tighter photometric distribution than the real blue edge in both colour-magnitude and colour-colour space. Since the Besancon model accounts for photometric error and reproduces the redder features of the CMD quite well, it is likely that this discrepancy is intrinsic to the model.

The Besancon model uses a halo comprised of a single stellar population which has a simple power law spatial distribution, a mean abundance of $[Fe/H] \sim -1.78$ and a metallicity dispersion of 0.5 dex. However, the numerous studies referenced in Sect. 1 indicate that simple models have difficulty reproducing the halo spatial distribution and demonstrate that the halo is partly, perhaps mostly, comprised of streams of stars stripped from objects during the hierarchical formation of the Milky Way. The stark difference in uniformity between the real and simulated blue edge argues against simple single-population models of the deep halo.

We also note that the simulated galaxy has a slightly different overall colour-colour distribution, with a gentler slope and a bluer cutoff in the $(U-B)_0$ colour distribution. This may not indicate a model deficiency as much as a mismatch between the real and simulated filters. Our observational data are calibrated to the standards of Landolt (1992) while the Besancon simulation is tied to the model atmospheres of Lejeune, Cuisinier & Buser (1997, 1998), which itself is tied to the observational plane by the calibration of Schmidt-Kaler (1982). It is unsurprising that some discrepancy would arise between two different calibrations.

[1] Available online at http://bison.obs-besancon.fr/modele/.

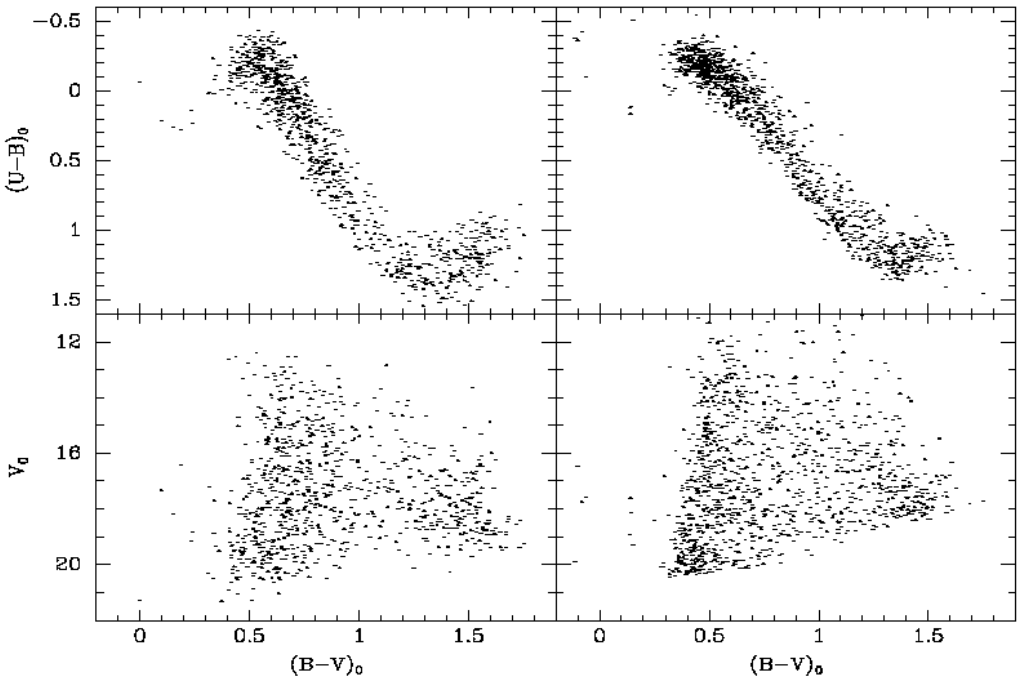

Figure 3. A comparison of the SA141 photometry (left panels) to the Besancon simulation (right panels). Note the much tighter blue edge population in the simulation.

3.3 Metal abundances and absolute magnitudes

The metal content of main sequence stars can be measured by the amount of line-blanketing absorption affecting their ultraviolet photometry. Low metal abundance produces weak atmospheric absorption lines and increased ultraviolet emission, or ultraviolet excess (UVX; Wildey et al. 1962).

Sandage (1969) detailed a technique for using the UVX – as measured through UBV photometry – to measure approximate abundances. The method determines the two-colour location of a star with reference to iso-metallicity ridgelines. The UVX measure, $\delta(U-B)$, is the difference between each star's $(U-B)_0$ colour and that of a metal-rich star of identical $(B-V)_0$, with the reference population defined in this case by the Hyades sequence, which Cayrel, Cayrel de Strobel & Campbell (1985), Boesgaard & Friel (1990) and Taylor (1998) estimate has an abundance between $[Fe/H]$=+0.10 and $[Fe/H]$=+0.13. We adopt an abundance of +0.13 dex for our analysis.

Figure 5 shows the de-reddened two-colour, $(U–B)_o$–$(B–V)_o$ of the SA 141 stars that fall within the colour range of the Karatas & Schuster (2006) UVX calibration. The solid lines indicate the metal content, ranging for the reddest line, which is a metal-rich line from the Hyades sequence, to the bluest line, which indicates the maximum underabundance envelope defined by Sandage (1969).

Inspection of Fig. 5 shows that the stars at bluer $(B-V)_0$ colours tend to lie along the more metal-poor lines while redder stars tend to lie along the more metal-rich lines. This is in keeping with expectations of standard Galactic structure models. The redder stars are intrinsically faint and nearby, in regions dominated by the metal-rich thin disk. The bluer stars are intrinsically bright and distant, in regions dominated by the metal-poor halo. A significant number of faint blue halo stars lie beyond the most metal-poor line, which corresponds to $[Fe/H]$=−2.23 in the calibration of Karatas & Schuster (2006). This could represent the low-metallicity tail of the halo but would also represent photometric scatter and evolved stars that have colours outside the main sequence locus. A smaller number of nearby red disk stars lie redward of the Hyades line, possibly representing the high-metallicity tail of the disk. Excluding the outlying stars from analysis can lead to a systematic bias, which we address in Sect. 4.2.

To derive $[Fe/H]$ abundances, we first measure $\delta(U-B)$, the colour difference between each star and the maximum metallicity line. This measure is then transformed to $\delta_{0.6}$, the UVX measure normalized to a $(B-V)_0$ colour of 0.6 (where $\delta(U-B)$ reaches its peak value) along the indicated iso-metallicity ridgelines. Eight constant-abundance lines of Sandage (1969), drawn in Fig. 5, have been used to transform the $\delta(U–B)$ measures of our stellar sample into normalized $\delta_{0.6}$ measures. Constant-metallicity lines are scaled as a fraction of the maximum line-blanketing "M" value in increments of 0.125. The lines are taken from Table 1A of Sandage with adjustments as detailed in equations (2)−(4) of Karatas & Schuster (2006).

We convert the $\delta_{0.6}$ measures to approximate abundances using the Karatas & Schuster (2006) relation:

$$[Fe/H] = +0.13(\pm0.04) - 4.84(\pm0.60)\delta_{0.6} - 7.93(\pm2.24)\delta_{0.6}^2 \quad (1)$$

This relation is valid for the ranges of $+0.41 \leqslant [Fe/H] \leqslant$

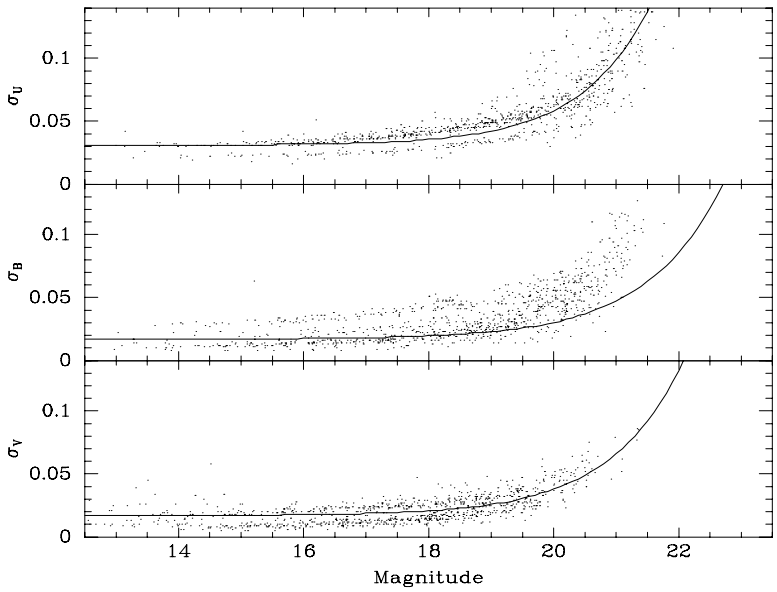

Figure 4. Error measurements for stars from the SA141 field. The error trends show multiple loci owing to the varying quality of the data. The solid line represents the error function of the simulated data.

-2.23, $-0.04 \leqslant \delta_{0.6} \leqslant +0.29$ and $0.3 \leqslant (B-V)_0 \leqslant 0.9$. 368 of the SA 141 stars fall within this parameters space.

Absolute magnitudes of program stars are then estimated with the following relation of Karatas & Schuster (2006):

$$M_V = 2.77 + 4.38(B{-}\mathrm{V})_\circ^2 - 48.98\delta_{0.6}^2 + 219.75(B{-}\mathrm{V})_\circ\ \delta_{0.6}^2 - 198.93(\mathrm{B{-}V})_\circ^2\ \delta_{0.6}^2 + 11.04(B{-}\mathrm{V})_\circ^3\ \delta_{0.6} \quad (2)$$

Abundance uncertainties are calculated by propagating the photometric uncertainties through the relevant equations. The abundance uncertainties are large, starting at a mean 0.2−0.3 dex for nearby ($z < 4$ kpc) stars, reaching 0.5 dex at 8 kpc and 0.7−0.8 dex at 15 kpc. This indicates that the abundance distribution of the thin and thick disks should be well-constrained. However, the deep halo, where the number of stars is low and the photometric uncertainties high, may be poorly constrained, an issue we address in Sect. 4.2.

Our measurement of stellar abundances, absolute magnitudes and distances is predicated on the assumption that these stars are all main sequence stars. This is not the case and some degree of contamination from evolved stars is expected. The evolved stars will be more distant than the main sequence stars and consequently more metal-poor, given the abundance distribution identified by previous investigators and constrained in Sect. 4. This may cause analysis of the nearby sample to skew metal-poor.

Fortunately, the Besancon simulated galaxy retains information on luminosity class. To evaluate the effect of this on our derived abundance distribution, we ran the simulated galaxy through our analysis pipeline and examined UVX-based metallicity measures as a function of midplane height, both with evolved stars removed from the sample and with evolved stars retained and evaluated as though they were main sequence stars. We found that retaining the evolved stars caused a small metal-poor skew in the derived metallicity that had a maximum of −0.1 dex but was generally around a few 0.01 dex. The reason the effect is so small is that while the evolved stars comprise 10-20% of the star-counts at any magnitude, a significant number lie outside the maximum and minimum UVX boundaries shown in Fig. 5 and are rejected on that basis. Indeed, it is likely that some of the outliers in Fig. 5 are, in fact, evolved stars. Additionally, the relatively blue cutoff of our abundance and absolute magnitude calibrations removes the redder stars where the luminosity difference between giant and dwarf is larger and the contamination is therefore from far more distant and more metal-poor stars. We have chosen not to remove the evolved star bias as it is smaller than the abundance uncertainties.

4 METALLICITY DISTRIBUTION

4.1 Raw Abundance Gradients

The trend of mean metal abundance $< Fe/H] >$ against $< z >$ height above the Galactic plane is shown in Figure 6 and detailed in Table 1. Mean metal abundances are derived from maximum likelihood Gaussian fits for star numbers and z intervals given in Table 1. As can be seen in Figure 6, at distance of $z < 4$ kpc – where the S02 and Robin et al. models indicate that the thin and thick disks dominate – there is a vertical abundance gradient of approximately $d[Fe/H]/dz = -0.15$ dex kpc^{-1}. At distance beyond 5 kpc

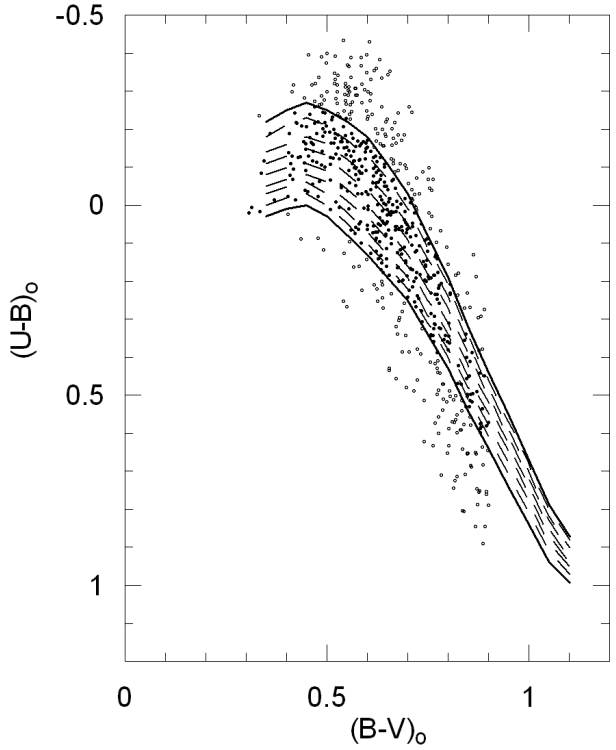

Figure 5. $(U–B)_o$-$(B–V)_o$ two-colour diagram for stars in SA 141 field. Standard relations for the Hyades and for the metal-poor lines of $(U–B)_{0.25M}$, $(U–B)_{0.50M}$, $(U–B)_{0.75M}$, and $(U–B)_M$ (metal-free) from Sandage (1969) are drawn as solid lines. Intermediate metal-poor lines of $(U–B)_{0.125M}$, $(U–B)_{0.375M}$, $(U–B)_{0.625M}$, $(U–B)_{0.875M}$ are drawn as dashed lines. The decimal fractions indicate the proportion of the maximum ultraviolet excess, which corresponds to zero metallicity. Open points are stars that fall outside of our constrained abundance range.

– where the halo begins to dominate – the metallicity measures are less precise but are consistent with a flattening of the abundance gradient (0.03−0.06 dex kpc^{-1}). At large distances (> 12 kpc), the abundance seems to *rise* slightly. However, the data at these faint magnitudes suffers from low completeness levels and it is likely that this reflects a bias near the magnitude limit or contamination from evolved horizontal branch (HB) stars (Sections 4.2 and 4.3).

4.2 Debiasing and Deconvolving the Abundance Distribution

The raw mean abundances shown in Figure 6 can not be taken at face value due to two complicating factors. First, the vertical abundance distribution is a convolution of the intrinsic abundance and density distributions of the component populations. Second, the method itself induces bias. Our metallicity calibration only extends from $[Fe/H] = +0.41$ to $[Fe/H] = -2.23$. This cuts off the low-metallicity tail of the halo and the high-metallicity tail of the disk – a process shown visually in Figure 5. Removing these outlying stars results in a systematic bias.

The dramatic effect of this bias can be demonstrated by applying our UVX analysis pipeline to the Besancon simulated data. Figure 7 compares the simulated abundances

Table 1. Mean metal abundances for z intervals (Column 1). Column 2 shows the mean $< z >$ of the stars in each bin while Columns 3 and 4 show the mean $< [Fe/H[>$ and uncertainty of the mean, respectively. Column 5 indicates the calculated abundance dispersion of the stars while Column 6 indicates the number of stars in each bin.

z range	$< z >$	$< [Fe/H] >$	$\sigma_{<[Fe/H]>}$	$\sigma_{[Fe/H]}$	N
[0, 1]	0.64	-0.50	±0.07	0.56	75
(1, 2]	1.48	-0.61	±0.06	0.55	116
(2, 3]	2.47	-0.79	±0.12	0.59	43
(3, 4]	3.53	-0.93	±0.11	0.28	31
(4, 5]	4.52	-0.65	±0.17	0.48	23
(5, 6]	5.38	-0.96	±0.21	0.60	18
(6, 7]	6.52	-0.95	±0.23	0.31	12
(7, 8]	7.34	-0.55	±0.24	...	9
(8, 9]	8.52	-1.23	±0.35	...	8
(9, 10]	9.38	-1.13	±0.29	...	9
(10, 11]	10.54	-0.99	±0.33	...	7
(11, 13]	12.31	-0.27	±0.25	...	9
(13, 15]	14.02	-0.43	±0.20	...	11
[15, 21]	16.73	-0.50	±0.39	...	7

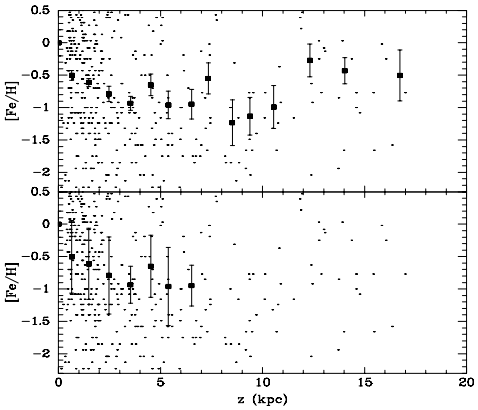

Figure 6. Relation between $< [Fe/H] >$ and $< z >$ for the range of $0 \leqslant z \leqslant 20$. There is a slight metallicity gradient $d[Fe/H]/dz = -0.15$ dex kpc^{-1} for $z < 4$ kpc, where the thin and thick disks dominate. Error bars in the top panel reflect the formal uncertainty in the mean calculated by maximum likelihood from the input photometric errors. Error bars in the bottom panel reflect the measured intrinsic abundance dispersion.

with the UVX-derived abundances. While the two scales follow each other closely at the metal-rich end, the trend veers at low abundances. The reason is that the metal-poor halo stars have a large abundance dispersion – both intrinsic (the Besancon halo has a 0.5 dex dispersion) and observational (0.5−0.8 dex from the UBV photometric uncertainties propagated through the UVX equations). The low-abundance cutoff removes the (intrinsic plus photometric scatter) low-metallicity tail of this distribution, while leaving the high-metallicity tail intact. In the faintest reaches of our halo sample, this shifts the derived mean abundance by as much as 0.4 dex.

Figure 8 contrasts the underlying intrinsic mean abundance distribution against the UVX-derived mean abundance distribution. The difference between the two is stark

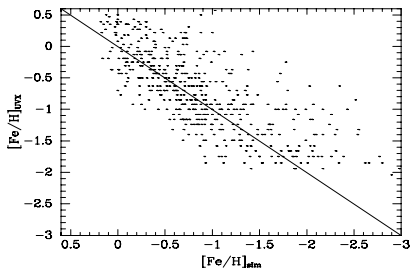

Figure 7. A demonstration of the bias induced by our UVX analysis. The points show the input abundances from the Besancon simulation contrasted against those derived from the UVX pipeline and simulated UBV photometry. The line represents unity. The sudden shift of the low abundances away from unity is not the result of miscalculation or error but the increase in dispersion combined with the removal of the metal-poor measures whose UVX properties lie beyond the last ridgeline in Figure 5.

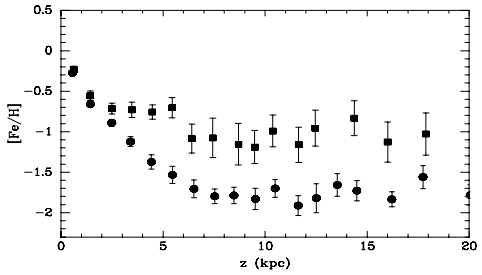

Figure 8. A demonstration of the metallicity bias induced by UVX analysis. The circles represent the intrinsic mean abundance distribution of the Besancon simulated data. The square points represent the *derived* mean abundance measures from the simulated UBV photometry. In both cases, the uncertainties are calculated from maximum likelihood (with an assumed uncertainty of $\sigma_{Fe/H} = 0.2$ for the intrinsic abundances). Because the UVX method has large uncertainties at faint magnitudes and only extends to $[Fe/H] = -2.23$, a significant metal-rich bias is induced when the stars scattered to low abundances are removed, as demonstrated in Figure 7.

and is the result of the abundance cut-off. A similar bias occurs for the metal-rich thin disk, but is not as dramatic owing to the smaller uncertainties for the bright disk stars and the smaller (0.2 dex) intrinsic dispersion of thin disk abundance. Note also that the error bars in Figure 8 are smaller than those of Figure 6, owing to the larger number of faint halo stars in the real data.

Untangling the halo metallicity distribution under these circumstances is beyond the scope of this paper –and may indeed be impossible if the halo metallicity distribution is *not* a simple single population but, as seems likely, comprised of multiple components and/or stream of stars. However, since (a) the SA 141 data and UVX calibration are on the same photometric system (both are tied to the Landolt standards) and; (b) the nature of the low-metallicity bias is *known*, it is possible to construct toy models for comparison.

We constructed synthetic metallicity distributions by assuming the structural parameters detailed in S02, metallicity distributions from AP06 and R03 and a distance-uncertainty relation taken directly from the SA 141 data. Both formulations posit a halo and thick disk with no metallicity gradient and abundance dispersions of 0.3 and 0.5 dex, respectively. The AP06 mean metallicities are −0.68 and −1.4 dex for thick disk and halo, respectively. The corresponding R03 abundances are −0.78 and −1.78 dex. For the thin disk, we took the Besancon metallicity distribution, which is a combination of seven thin disks in which metallicity is dependent on age. The mean metallicity of the disks varies with age. However, the overall weighted mean abundance of the seven disks is $[Fe/H] = -0.08$ and the weighted weighted 1σ is 0.2 dex. We applied the low- and high-abundance cutoffs that are applied to the real data to replicate the bias.

Figure 9 shows the result of these comparisons. What is striking about the distributions is that the photometric properties of the Galactic populations show a rough distribution consistent with the models, but overlayed with several metal-rich outlying data points (at 4.5, 7.5 and beyond 12 kpc). S02 (and many studies cited therein and in Sect. 1) have suggested that the halo field star distribution has two components. The first is a uniform flattened metal-poor distribution; the second an irregular mass of star streams created during the hierarchical formation of the Milky Way (although Carollo et al. 2007, using the SDSS, argue for two distinct halo structures, only distinguishable beyond 10 kpc). If the halo did have a uniform structure overlayed with streams, the abundance distribution in a pencil-beam survey *might* look like Figure 9, with a uniform distribution occasionally interrupted by more metal-rich populations. Inspection of Figure 6 shows a hint of this at the outlying points, where the individual points seems to show a vague bimodality, although the scatter it too large to be certain.

Deep proper-motion and/or radial velocity surveys of SA 141 would be needed to test this suggestion. It remains possible that these data points merely reflect some inadequacy of the method. Nevertheless, if verified, it would demonstrate that the stellar streams identified so clearly in I08 can also be identified in smaller less-precise archival UBV data sets by their departure from the underlying uniform distribution.

If we assume that the metal-rich points are outliers above the general distribution, then the literature models successfully reproduce the observed abundance distribution. The Besancon model appears to provide a slightly better description of the thick disk while the AP06 model provides a slightly better description of the halo. The halo is not well-constrained enough to address a possible abundance gradient. A slight thick disk abundance gradient would bring the AP06 thick disk in line with the UVX results, albeit only because it would lower the mean abundance in the narrow range of z heights dominated by the thick disk.

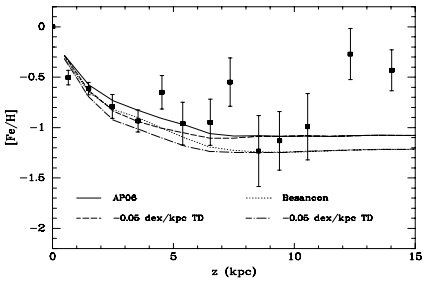

Figure 9. Comparison of the UVX-based abundances to those predicted by the Besancon and AP06 distributions (solid and dotted lines) as well as both distributions with a −0.05 dex/kpc abundance gradient in the thick disk (dashed and dot-dashed lines). In this figure, the model predictions do not correspond to the actual metallicity distribution, but to the *measured* abundance distribution, taking into account the bias induced by the UVX methodology.

4.3 Young Stars in the Halo?

Figure 10 shows the $[Fe/H]$, $(B–V)_o$ diagram overlayed with Yonsei-Yale (Y^2) isochrones of Yi, Kim &Demarque (2003). The turn-off loci from the isochrones are overlayed for ages of 6, 8, 10, 12, and 14 Gyr, assuming $[\alpha/Fe] = +0.30$. While the vast majority of the stars in SA141 have photometric properties consistent with ages greater than 12 Gyr, a handful of metal-rich stars are bluer than the old turnoff. These stars are all beyond 6 kpc and would have implied ages less than 10 Gyr. A young metal-rich population of stars is unexpected given previous spectroscopic and photometric surveys of the halo (see Carollo et al. 2007).

None of the stars comprising this young population have particularly large photometric errors. Nor are they concentrated in one part of the SA 141 field, eliminating the possibility that they are compromised by bad pixels or nearby saturated stars. Although the abundance uncertainties are large for the fainter stars (0.5-0.8 dex) and they suffer from the aforementioned metal-poor bias, the mean abundance is clearly metal-rich (-0.2 with a dispersion of 0.7).

These stars are unlikely to represent the halo streams to which we ascribe the outlier points in Figures 6 and 9. Halo stream stars are generally thought to be metal-poor – as reflected in the blue, metal-poor (BMP) stars described in Preston, Beers & Shectman (1994), Carney et al. (1996) and Unavane, Wyse & Gilmore (1996). While some streams, most notably those of the merging Sagittarius dSph, are known to be slightly more metal-rich than the halo (Sbordone et al. 2004; Martinez-Delgado et al. 2005; Chou et al. 2007), our distant SA 141 stars are not clumped in distance, as would be expected for a tidal stream.

It's possible that these stars are blue straggler stars (Carney, Latham & Laird 2005) although there is no reason to believe that blue stragglers would be so much richer than the canonical halo. However, the most likely explanation is that these are contaminating HB stars. Figure 11 shows the SA 141 UBV diagram with the young stars of Figure 10 marked as large circles. To contrast their location against that of HB stars, we have generated a synthetic HB from the Dartmouth Stellar Evolution Database (Dotter et al. 2007), assuming an abundance of $[Fe/H] = -1.5$, [α/Fe]=+0.2, an age of 12 Gyr and mass loss of 0.05 ± 0.05 M_o[2]. It can be seen that the HB somewhat overlaps the metal-rich end of MS in colour-colour space. If the distant blue metal-poor "young" stars were on the HB, rather than the MS, they would be spread over distances of 25−150 kpc, a distance range dominated by the extremely metal-poor ($[Fe/H] \sim -2.2$) outer halo described by Carollo et al. (2007). We find this the most likely explanation for these outlying stars. Spectroscopy or proper motions of these stars would be able to determine their nature.

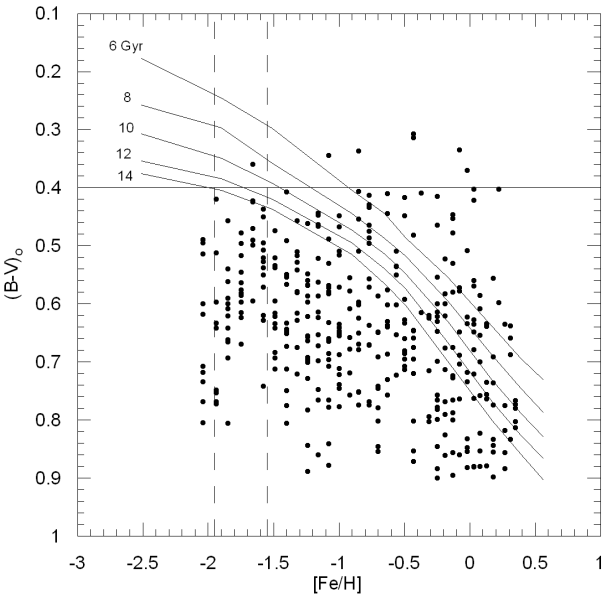

Figure 10. (a) The $[Fe/H]$, $(B–V)_o$ plot for the 368 stars in SA 141 field. The turn-off loci from the isochrones of Yi et al. (2003) are plotted for the ages of 6, 8, 10, 12, and 14 Gyr, with $[\alpha/Fe] = +0.30$. The lines indicate the young metal-poor stars surveyed by Unavane et al.

5 CONCLUSIONS

We have performed an analysis of the ultraviolet excesses of stars in the SA141 field. We find that photometric uncertainties propagate very quickly into large (0.5−0.8 dex) abundance uncertainties. These uncertainties can cause systematic biases at the low-metallicity end of the UVX calibration. These biases must be properly accounted for when probing the ensemble properties of the field stars. Specifically, the limitation of the method to stars more metal rich than $[Fe/H] = -2.23$), when combined with the intrinsic abundance dispersion of the halo and the necessarily large UVX-abundance uncertainties at faint magnitudes, induces a systematic bias in our analysis of the population abundance. This bias can be modeled and corrected if assumptions are made about the underlying metallicity distribution.

[2] The location of the SHB is only sensitive to the input parameters at colours bluer than the colour range over which we measure UVX abundances.

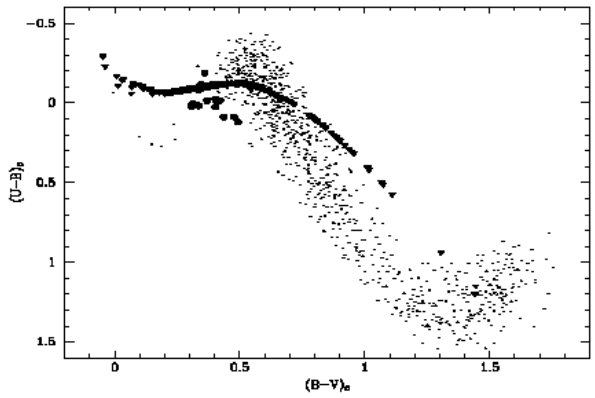

Figure 11. A analysis of the unusual halo stars. The dots show the UBV photometry of the SA141 field stars. The large circles are the outlying apparently young stars from Fig. 9. The triangles are a synthetic horizontal branch. Note the overlap of the HB and MS sequences where the outlying stars are found.

The inferred abundance distribution is roughly consistent with the metallicity distribution depicted in I08 as well as the spectroscopic study of AP06 and the simulations of R03. However, there are a number of outlying data points that could indicate contamination of the SA 141 field by more metal-rich halo streams.

We identify a trace population of apparently young metal-rich halo stars. However, these are not associated with any of the outlier data points and we find it is most likely that these objects are halo HB stars that have photometric properties similar to metal-rich MS stars.

To exploit future UBV data-bases, it will be necessary to refine the calibration of the UBV ridgelines based on up-date photoelectric data calibrated to the Landolt system as well as to probe the UBV properties of very metal-poor stars to extend the metallicity range of the calibration. This would allow the abundance distribution of the distant halo to be explored with more precision and confidence to test models of Galactic formation and unravel the fine structure of the Galactic halo and thick disk.

6 ACKNOWLEDGMENTS

We thank Annie Robin, the referee, for her useful and constructive comments concerning the manuscript.

REFERENCES

Allende Prieto C., Beers T. C., Wilhelm R., Newberg H. J., Rockosi C. M., Yanny B., & Lee Y. S., 2006, ApJ, 636, 804 [AP06]
Belokurov V. et al., 2006, ApJ, 642, L137
Boesgaard A. M., & Friel E. D., 1990, ApJ, 351, 467
Cambresy, L.,Jarrett, T. H., Beichman, C. A., 2005, A&A, 435, 131
Carollo D. et al., 2007, Nature, 450, 1020
Carney B., Laird J.B., Latham, D.W., Aguilar L., 1996, AJ, 112, 668
Carney B.W., Latham D.W., Laird J.B., 2005, AJ, 129, 466
Cayrel R., Cayrel de Strobel G., & Campbell B. 1985, A&A, 146, 249
Chen B. et al., 2001, ApJ, 553, 184
Chou M.-Y. et al., ApJ, 670, 346
Dotter A., Chaboyer B., Jevremović D., Baron E., Ferguson J. W., Sarajedini A., & Anderson J., 2007, AJ, 134, 376
Du C.-h., Zhou X., Ma J., Shi J.-R., Chen A. B.-C., Jiang Z.-J., & Chen J.-S., 2004, AJ, 128, 2265
Eggen O.J., Lynden-Bell D., Sandage A.R., 1962, ApJ, 136, 748
Fan X., 1999, AJ, 117, 2528
Freeman K. & Bland-Hawthorn J., 2002, ARA&A, 40, 487
Gilmore G., Wyse R.F.G., 1985, AJ, 90, 2015
Grillmair C. J., 2006, ApJ, 645, L37
Ivezić Ž. et al., 2000, AJ, 120, 963
Ivezić Ž. et al., 2008, ApJ, 684, 287 [I08]
Jurić M. et al., 2008, ApJ, 673, 864
Karaali S., Ak S.G., Bilir S., Karataş Y., Gilmore G., 2003, MNRAS, 343, 1013
Karataş Y., Schuster, W.J., 2006, MNRAS, 371, 1793
Karataş Y., Kilic M., Guneş O. & Limboz F., 2008, PASP, *eprint arXiv.0809.2486*
Landolt A.U., 1992, AJ, 104, 340
Lejeune T., Cuisinier F., & Buser R., 1997, A&AS, 125, 229
Lejeune T., Cuisinier F., & Buser R., 1998, A&AS, 130, 65
Majewski S. R., 1992, ApJS, 78, 87
Majewski S. R., 1993, ARA&A, 31, 575
Majewski S.R., Munn J. A., & Hawley S. L., 1996, ApJ, 459, L73
Majewski S.R., Skrutskie M.F., Weinberg M.D., & Ostheimer J.C., 2003, ApJ, 599, 1082
Marin-Franch A. et al. 2008, ApJ, *eprint arXiv.0812.4541*
Martínez-Delgado D., Butler D.J., Rix H.-W., Franco V. I., Peñarrubia J., Alfaro E. J., & Dinescu D. I., 2005, ApJ, 633, 205
Monet D.G. et al., 1996, USNO-SA2.0, (Washington: US Naval Observatory)
Newberg H.J. et al., ApJ, 569, 245
Norris J., 1987, ApJ, 314, L39
Preston G.W., Beers T.C., Shectman S.A., 1994, AJ, 108, 538
Reid I. N., Yan L., Majewski S., Thompson I., & Smail I., 1996, AJ, 112, 1472
Richards G.T. et al., 2001, AJ, 121, 2308
Robin A. C., Reylé C., Derrière S., & Picaud S., 2003, A&A, 409, 523 [R03]
Rocha-Pinto H. J., Majewski S. R., Skrutskie M. F., Crane J. D., & Patterson R. J., 2004, ApJ, 615, 732
Roman N.G., 1954, AJ, 59, 307
Sandage, A., 1969, ApJ, 158, 1115
Sbordone L., 2004, *astro-ph/0411002*
Schlegel D.J., Finkbeiner D.P., Davis M., 1998, ApJ, 500, 525
Schmidt-Kaler Th., 1982, in: Landolt-Borstein, Neue Serie, Gruppe VI, Bd. 2b, Schaifers K., Voigt H.H. (eds.). Springer, Berlin Heidelberg New York, p. 14
Searle L., Zinn R., 1978, ApJ, 225, 357
Siegel M.H., Majewski S.R., Reid I.N., Thompson I.B., 2002, ApJ, 578, 151 [S02]
Siegel M.H., Majewski S.R., Sohn S.T., Shetrone M.D. & Patterson R. J., ApJ, *submitted*

Smith J.A., Tucker D.L., Kent S. et al, 2002, AJ, 123, 2121
Taylor B.J. 1998, PASP, 748, 708
Trefzger C.F., Pel J.W., & Gabi S., 1995, A&A, 304, 381
Unavane M., Wyse, R.F.G., Gilmore G., 1996, MNRAS, 278, 727
Vivas A.K. et al., 2001, ApJ, 554, L33
Vivas A.K., & Zinn R., 2006, AJ, 132, 714
Wildey R.L., Burbidge E.M., Sandage A.R., & Burbidge G.R., ApJ, 135, 94
Yanny B. et al., 2000, ApJ, 540, 825
Yanny B. et al., 2003, ApJ, 588, 824
Yi S.K., Kim Y.C., Demarque P., 2003, ApJS, 144, 259
Yoss K.M., Neese, C.L., & Hartkopf W.I., 1987, AJ, 94, 1600.